Dependent component analysis-based approach to robust demarcation of the skin tumors

Ivica Kopriva[*a*], Antun Peršin[a], Neira Puizina-Ivić[b], Lina Mirić[b]
[a]Division of Laser and Atomic Research and Development, Ruđer Bošković Institute, Bijenička cesta 54, P.O. Box 180, 10002, Zagreb, Croatia
[b]Clinic of Dermatovenerology, Clinical Hospital and School of Medicine, Šoltanska 1, 21000 Split, Croatia

ABSTRACT

Method for robust demarcation of the basal cell carcinoma (BCC) is presented employing novel dependent component analysis (DCA)-based approach to unsupervised segmentation of the red-green-blue (RGB) fluorescent image of the BCC. It exploits spectral diversity between the BCC and the surrounding tissue. DCA represents an extension of the independent component analysis (ICA) and is necessary to account for statistical dependence induced by spectral similarity between the BCC and surrounding tissue. Robustness to intensity fluctuation is due to the scale invariance property of DCA algorithms. By comparative performance analysis with state-of-the-art image segmentation methods such as active contours (level set), K-means clustering, non-negative matrix factorization and ICA we experimentally demonstrate good performance of DCA-based BCC demarcation in demanding scenario where intensity of the fluorescent image has been varied almost two-orders of magnitude.

Keywords: basal cell carcinoma, photodynamic detection, dependent component analysis, tumor demarcation, multi-spectral image.

1. INTRODUCTION

Among the skin tumors, basal cell carcinoma (BCC) accounts for about 80% of all non-melanoma skin cancers [1]. Increased occurrence of the skin cancer all over the world, [2], implies the large need for complementary methods for detection and accurate demarcation of these skin cancers at an early stage to limit the damage caused by the tumors [3]. Photodynamic diagnoses (PDD) is a method for tumor demarcation that is based on the visualization of a fluorophore, with the ability to accumulate in tumor tissue, by the use of fluorescence imaging. A photosensitiser widely used in clinical applications is δ-5 aminolevulinic acid (ALA) induced protoporphyrin IX (PpIX) [1,3-8]. ALA is a non-fluorescent precursor of fluorescent PpIX, with a degree of selective accumulation shown in a variety of malignancies [9]. Thus, by using suitable intensity excitation light, the PpIX can be located in the tissue by virtue of its fluorescence. Visualization of the PpIX represents the basis of the PDD of the skin tumors and has been exploited in the design of the fluorescence imaging systems [1,4-8,10]. Image processing methods widely used for the optical diagnoses, i.e. demarcation, of the BCC after administration with ALA induced PpIX are ratio imaging method [1,4,6], and threshold based imaging [3]. As it has been previously demonstrated in [11], accuracy of both methods in tumor demarcation essentially depends on the optimality of the threshold that up to some extent is defined heuristically. When intensity of the fluorescence image is fluctuating the threshold based methods will introduce errors in tumor demarcation, what has been demonstrated in [11], where unsupervised decomposition of the red-green-blue (RGB) fluorescent image of the tumor, for the BCC demarcation purpose, has been performed by using independent component analysis (ICA) [12,13]. ICA is already relatively old theory derived over last almost 20 years for unsupervised analysis of the multivariate data sets. Of the interest for tumor demarcation is the capability of ICA algorithms for unsupervised segmentation of multi-spectral and hyper-spectral images [14,15]. Unsupervised segmentation by ICA is based on assumption of statistical independence among the objects resident in the multi-spectral fluorescent image of the tumor, where BCC is one object

[*] ikopriva@gmail.com; phone +385 1 4571 286; fax +385 1 4680 104

Medical Imaging 2009: Image Processing, edited by Josien P. W. Pluim, Benoit M. Dawant,
Proc. of SPIE Vol. 7259, 72594Q · © 2009 SPIE
CCC code: 1605-7422/09/$18 · doi: 10.1117/12.806404

and surrounding healthy tissue is another object. Because statistical independence is scale invariant, it is expected that ICA will be robust with respect to the variation of the intensity level. This robustness should be of the interest in the early stages of the tumor development, in which case detection and accurate demarcation is of special importance [3]. We shall demonstrate that in the case of the low-dimensional multi-spectral images, such as RGB image for example, statistical independence assumption among the objects resident in the image scene is violated due to the overlapping of the spectra of the objects. Thus, coarse spectral resolution of the RGB image causes partial statistical dependence between the objects in the spatial domain and deteriorates performance of the ICA-based approach to tumor demarcation problem. In this paper we apply concept of dependent component analysis (DCA), [16-21], to fix the statistical dependence problem systematically by combining the linear preprocessing transform and ICA in transformed domain where statistical independence among the objects resident in the fluorescent multi-spectral image is increased. The main objective of this paper is experimental demonstration of the capability of the DCA-based multi-spectral image segmentation to yield an accurate estimate of the tumor demarcation line under high degree of variability of the intensity of the fluorescent image. This should lay down foundation for the design of the autonomous systems capable for robust calculation of the tumor demarcation lines in the real world clinical conditions.

2. MATERIALS AND METHODS

2.1 Patients

A patient with histologically verified diagnoses of basal cell carcinoma in the arm was admitted in Outpatient department of dermatovenerology in the Clinic of Dermatovenerology, Clinical Hospital Split. The study protocol, patient information and consent forms were approved by an independent ethics committee before patient was enrolled in the study. The ALA cream was prepared at the hospital pharmacy. It consisted of 20% 5-ALA-HCl (Medac, Hamburg, Germany) in an oinment base (Belobaza, Belupo, Koprivnica, Croatia), 2% of dimethylsulfoxide (DMSO) and 2% of edetic acid disodium salt (EDTA) (Titriplex III, Merck, Germany). The cream was prepared daily just prior the application. After cleaning the area with a saline solution, the cream has been applied to a thickness of approximately 1 mm covering the treated area and 1 cm of the surrounding skin. The area was covered by plastic occlusive dressing (Tegaderm, 3M, UK) and an aluminum foil on the top in order to protect treated skin from exposure to environment light. Before imaging, the occlusive dressing was removed and cream was wiped off gently with gauze. After imaging, disinfection of treated area was done and demarcation line was marked by tissue marking dye (TBS, Triangle Biomedical Sciences, Inc., Durham, NC, USA). Thereafter, surgical excision was obtained and specimen was fixed in 10% formalin and sent in the Laboratory for dermatopathology.

2.2 Fluorescence imaging

Fluorescence imaging has been performed by apparatus consisting of commercial RGB digital camera with precise manual focusing capability and illuminator. Illuminator is based on the cluster of light emitting diodes arranged circularly around camera lens and emitting in the range of 405 nm, which matches the absorption spectrum of PpIX. The fluorescence emission spectrum of PpIX has a dominant peak at 635 nm. Both spot diameter and fluorescence intensity can be adjusted independently in the range of 2 to 100 cm and 0.01 to 100 mw/cm^2, respectively. Depending on spot size and intensity applied, exposure time for capturing fluorescence images ranges from 0.01 to 10 sec. RGB image can be considered as multi-spectral image with the coarse spectral resolution. It is suitable for the application of the multivariate data analysis methods such as ICA and DCA in order to achieve unsupervised extraction of the BCC spatial map. This holds true as long as the fluorescent image consists of three or less objects. For the sake of illustration Figure 1a shows RGB image of the tumor illuminated with maximal intensity, Figure 1b shows RGB image of the tumor illuminated with intensity that was 9.15 times lower than the maximal intensity, Figure 1c shows RGB image of the tumor illuminated with the intensity that was 58.7 times lower that the maximal intensity, while Figure 1d shows RGB fluorescent image with demarcation line manually marked by the red line.

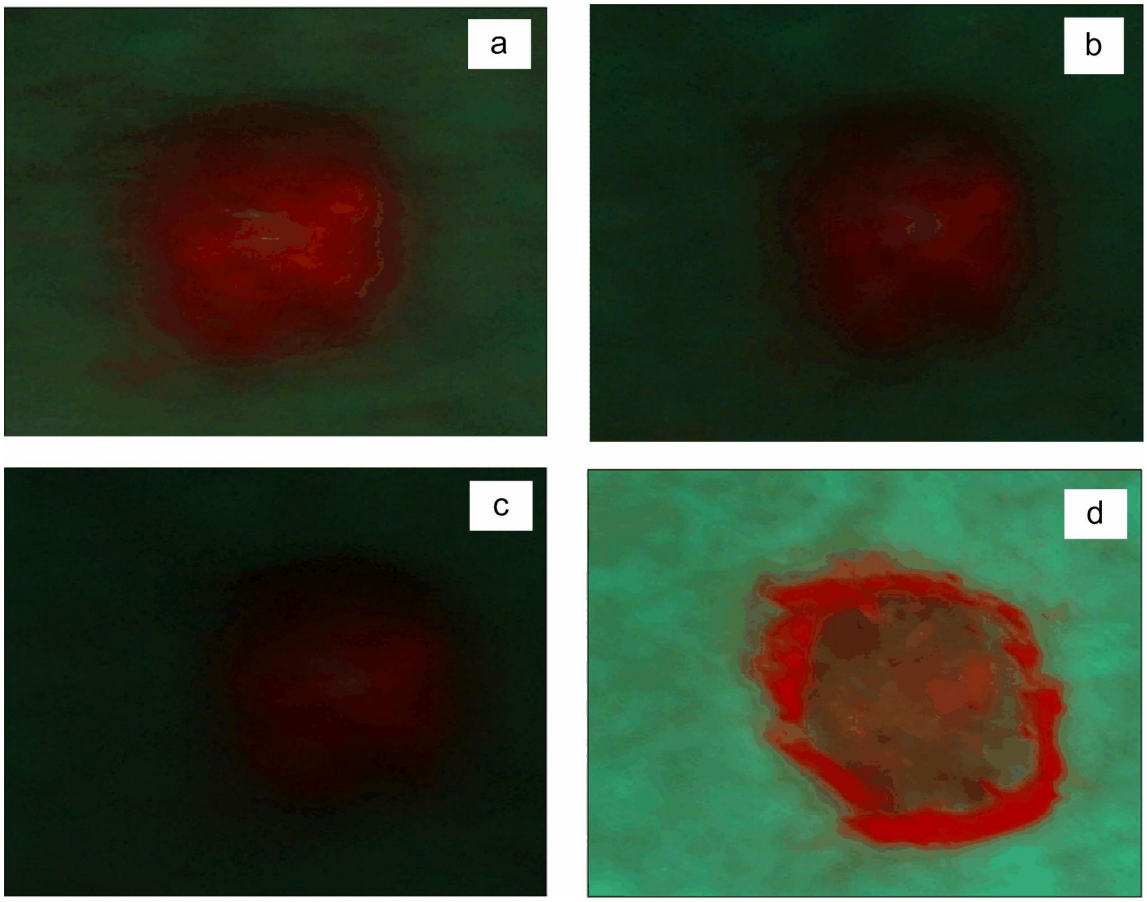

Fig. 1. (a) RGB fluorescent image of the BCC illuminated with the maximal intensity I_0; (b) RGB fluorescent image of the BCC illuminated with the intensity $I_0/9.15$; (c) RGB fluorescent image of the BCC illuminated with the intensity $I_0/58.7$; (d) RGB fluorescent image with demarcation line manually marked by the red line.

2.3 Multispectral imaging and dependent component analysis

For the segmentation purpose multi-spectral image is represented in a form of the static linear mixture model (SLMM) [11, 14, 15, 22-25]

$$\mathbf{X}=\mathbf{AS} \tag{1}$$

where $\mathbf{X}\in \mathrm{R}_{0^+}^{N\times T}$ represents multi-spectral image consisting of N spectral bands and $T=P\times Q$ pixels, $\mathbf{A}\in \mathrm{R}_{0^+}^{N\times M}$ represents basis or mixing matrix and $\mathbf{S}\in \mathrm{R}_{0^+}^{M\times T}$ represents matrix of the M objects or classes resident in the image scene. Each row of **X** and **S** is a signal or 1D image representation obtained from its 2D counterpart by some 2D→1D mapping. Most common type of mapping is the column- or row-stacking procedure also called vectorization. Because we are concerned with an unsupervised image decomposition problem, we have assumed **X**, **A** and **S** to be nonnegative, wherein both mixing matrix **A** and object matrix **S** must be estimated having at disposal multi-spectral image matrix **X** only.

The SLMM (1) is widely used in multi-spectral and hyper-spectral remote sensing, [14, 15, 22-25], where 3D image cube contains co-registered spectral images of the same scene. Within this application field, N represents the number of spectral bands; rows $\{\mathbf{x}_n\}_{n=1}^{N}$ of **X** represent spectral images, and columns of **X** represent multi-spectral pixel vectors at particular spatial locations, $t\le T$, in the image; T represents the number of pixels in the image, while column vectors $\{\mathbf{a}_m\}_{m=1}^{M}$ of the basis matrix **A** represent spectral responses of the corresponding objects $\{\mathbf{s}_m\}_{m=1}^{M}$, also called

sources, that themselves represent rows of **S**. Assuming that **X** represents an RGB image the number of spectral bands N equals 3. In order to relate the SLMM (1) to the image segmentation problem, we point out that sources $\{\mathbf{s}_m\}_{m=1}^{M}$ represent spatial maps of the objects resident in the image, while corresponding column vectors $\{\mathbf{a}_m\}_{m=1}^{M}$ of the basis matrix **A** represent their spectral responses. Following this interpretation we immediately see that spectral similarity of the objects $\mathbf{s}_m$ and $\mathbf{s}_n$ will affect the condition number of the basis matrix, because the corresponding column vectors $\mathbf{a}_m$ and $\mathbf{a}_n$ become collinear. When the objects have the same spectral response the column rank of the basis matrix is less than the number of objects M. Moreover, the corresponding objects become statistically dependent. This is easily verified by assuming that two objects $\mathbf{s}_m$ and $\mathbf{s}_n$ are spectrally very similar. Then $\mathbf{a}_n \cong c\mathbf{a}_m$, where c represents the intensity scaling factor. The contribution of these two objects at any pixel location t is: $\mathbf{a}_m s_{mt} + \mathbf{a}_n s_{nt} \cong \mathbf{a}_m s_{mt} + \mathbf{a}_m c s_{nt}$, implying that $\mathbf{s}_m$ and $c\mathbf{s}_n$ are indistinguishable, i.e., $\mathbf{s}_m$ and $\mathbf{s}_n$ are statistically dependent. Hence, fundamental requirement imposed by the ICA algorithms on the SLMM fails when objects, tumor and surrounding healthy tissue, become spectrally similar. This occurs for example when tumor is at an early stage of development. This spectral similarity problem presents a motivation to look for an extension of the basic ICA theory in order to achieve more accurate blind segmentation/separation of statistically dependent objects.

The basic idea behind ICA is to decompose a set of multivariate signals into a basis of statistically independent sources. In the unsupervised segmentation problem, which for the case of multi-spectral image is represented by SLMM (1), this implies estimation of the spectral reflectance matrix **A** and object matrix **S** having at disposal multi-spectral image **X** only. As already said, ICA solves related BSS problem under three assumptions made on the unknown source signal vector **s**: 1) each source signal is an independent identically distributed (i.i.d.) stationary random process; 2) the source signals are statistically independent at any position; and 3) at most one among the source signals has Gaussian distribution. The mixing matrix **A** although unknown is also assumed to be non-singular. Then the solution to the blind source separation problem (BSS) is obtained with the scale and permutation indeterminacy, i.e., $\mathbf{WA} = \mathbf{P\Lambda}$, where **W** represents the unmixing matrix, **P** is a generalized permutation matrix, and $\mathbf{\Lambda}$ is a diagonal matrix. These requirements ensure the existence and uniqueness of the solution to the BSS problem up to the ordering, sign and scale, [12,13]. Thus, ICA algorithms pose the scale invariance property what makes them attractive for the use in optical diagnosis of the BCC from the RGB fluorescence image when the absolute fluorescence level may vary from measurement to measurement.

However, we have shown that spectral similarity between the objects induces statistical dependence among them. Thus, one of the basic assumptions upon which the ICA theory is built on, statistical independence among the objects, is violated when they become spectrally similar. DCA represents an extension of the ICA in the solution of the BSS problem with statistically dependent sources. The strategy behind DCA is to find a linear transform T that can improve statistical independence between the sources **S** but leave the basis matrix **A** unchanged, i.e.,

$$T(\mathbf{X}) = T(\mathbf{AS}) \cong \mathbf{A}T(\mathbf{S}) \tag{2}$$

Linear transforms that possess such a required invariance property and generate less dependent sources in the new representation space include: high-pass filtering (HPF), [20]; innovation (Inn), [17]; and wavelet transforms (WT), [18, 19]. HPF can be seen as a special case of the innovations based preprocessing. This is because both innovations and HPF remove slowly varying part of the signal that is concentrated around DC component. In particular it has been already demonstrated in [13,17,18], that computationally very simple first order differentiator with the impulse response h=[1 -1] yields good performance in the image processing-type of applications. It has been used in our implementation of the DCA HPF algorithm in the experiments reported in Section 3.

Because the sources in the new representation space will be less statistically dependent, any standard ICA algorithm derived for the original BSS problem represented by the SLMM (1), can be used to learn the basis matrix **A**. Once the basis matrix **A** is estimated, the sources **S** are recovered by applying the pseudo-inverse of **A** on the multi-spectral image **X** in (1). In our experiments we have used enhanced version, [26], of the FastICA algorithm, [27, 28] due to its property of being asymptotically statistically efficient.

Nonnegative matrix factorization (NMF) algorithms, [29-32], can be viewed as a special class of the DCA algorithms, because they are also applicable to the SLMM (1) since the variables in the model are nonnegative. The NMF algorithms do not impose statistical independence and non-Gaussianity requirements on the sources. However, NMF algorithms generally require $N>>M$, which makes them not good candidate for unsupervised decomposition problems when **X** represents a low-dimensional multi-spectral image, such as RGB image, in which case N is small. Using a gradient descent approach to NMF yields multiplicative NMF algorithms [29,30,32]. They are known to be very

slowly convergent and easily get stuck in local minima. Therefore, in [31] an algorithm was recently derived that is based on the use of second-order terms, Hessian, in the Taylor expansion of a cost function to speed up convergence. Specifically, the NMF algorithm used in the experiments in the cited paper combines quasi-Newton optimization for basis matrix **A** and a fixed-point regularized least-square algorithm for **S**, with computer code provided in the appendix in [31]. Excellent performance of this algorithm has been demonstrated in [30,31]. We have used this NMF algorithm in the comparative experimental performance analysis presented in Section 3.

3. RESULTS

We have shown on Figures 1a to 1c RGB fluorescent images of the BCC illuminated with three different intensity levels, where intensity on Figure 1b was 9.15 times less than intensity on Figure 1a, and intensity on Figure 1c was 58 less than intensity in Figure 1a. Figure 1d shows RGB image of the BCC with manually drawn demarcation line. Through hystopathological analysis it has been verified that no tumor exists outside of the boundaries of this demarcation line. Figure 2a to 2c shows results obtained by applying statistically efficient version of the FastICA algorithm on Figures 1a to 1c, respectively. Equivalent results obtained by DCA-HPF algorithm are shown in Figures 3a to 3c. Evidently, performance of the ICA deteriorates when intensity, i.e. contrast, of the fluorescent image decreases. Figure 4 shows length of the demarcation lines, estimated from ICA- and DCA extracted spatial maps of the BCC as a function of the relative intensity of the illuminating light. The spatial maps were extracted by means of Canny's edge extraction method with a fixed threshold set to 0.5. The maximal intensity is represented by ratio 1.0 and minimal by ratio 58. Evidently, DCA algorithms yield stable estimate of the demarcation line despite the variability of the intensity of the fluorescence. Figure 5a shows tumor demarcation results obtained by applying the level set [33,34] clustering algorithm on the gray scale version of the RGB fluorescent image of the BCC shown in Fig. 1a, i.e. the image was acquired after illumination with the maximal intensity. Due to the weak boundaries between the tumor and surrounding healthy tissue the level set clustering method failed to converge toward true demarcation line. Figures 5b and 5c show tumor spatial maps extracted by K-means clustering [35] from the gray scale versions of the RGB fluorescent images of the BCC shown in Figures 1a and 1c. The interclass distance parameter was kept constant at the value 45 for both cases. Evidently the K-means clustering failed completely when intensity of the illuminating light was weak.

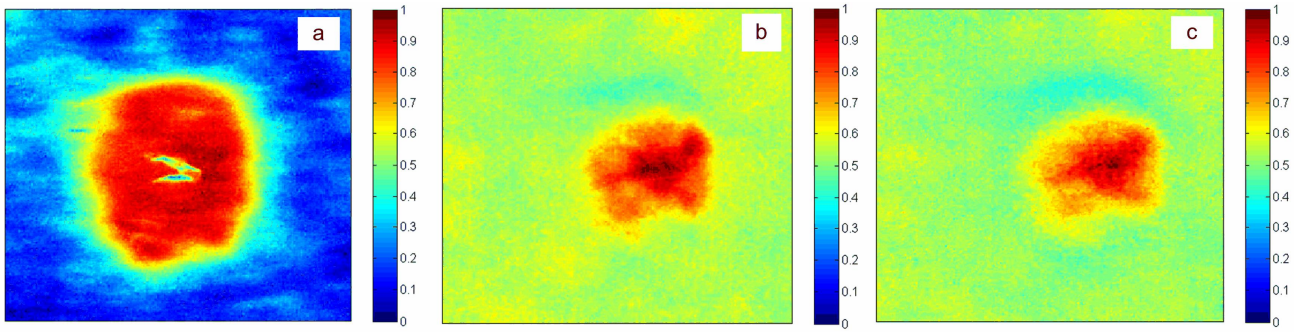

Fig. 2. BCC spatial maps extracted from fluorescent RGB images shown in Figures 1a, 1b and 1c by means of efficient FastICA algorithm. Extracted maps are normalized on interval [0, 1] and shown in pseudo-color scale.

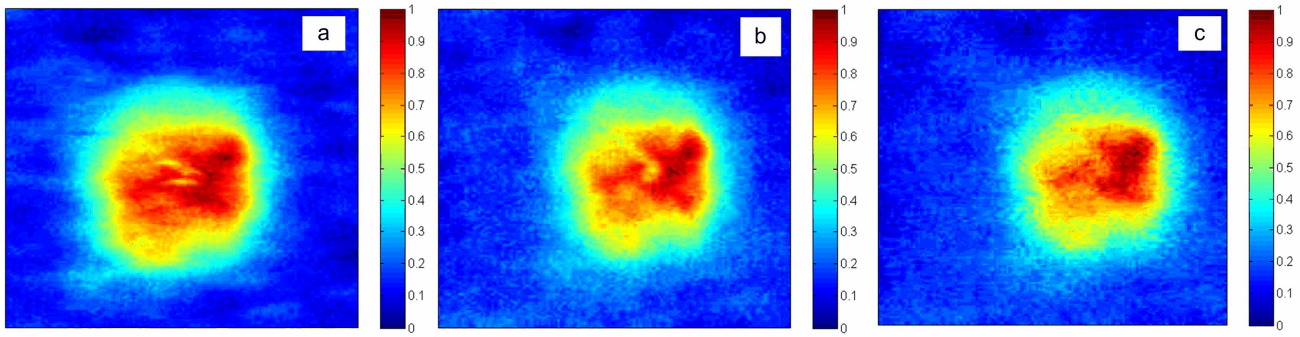

Fig. 3. BCC spatial maps extracted from fluorescent RGB images shown in Figures 1a, 1b and 1c by means of DCA-HPF algorithm. Extracted maps are normalized on interval [0, 1] and shown in pseudo-color scale.

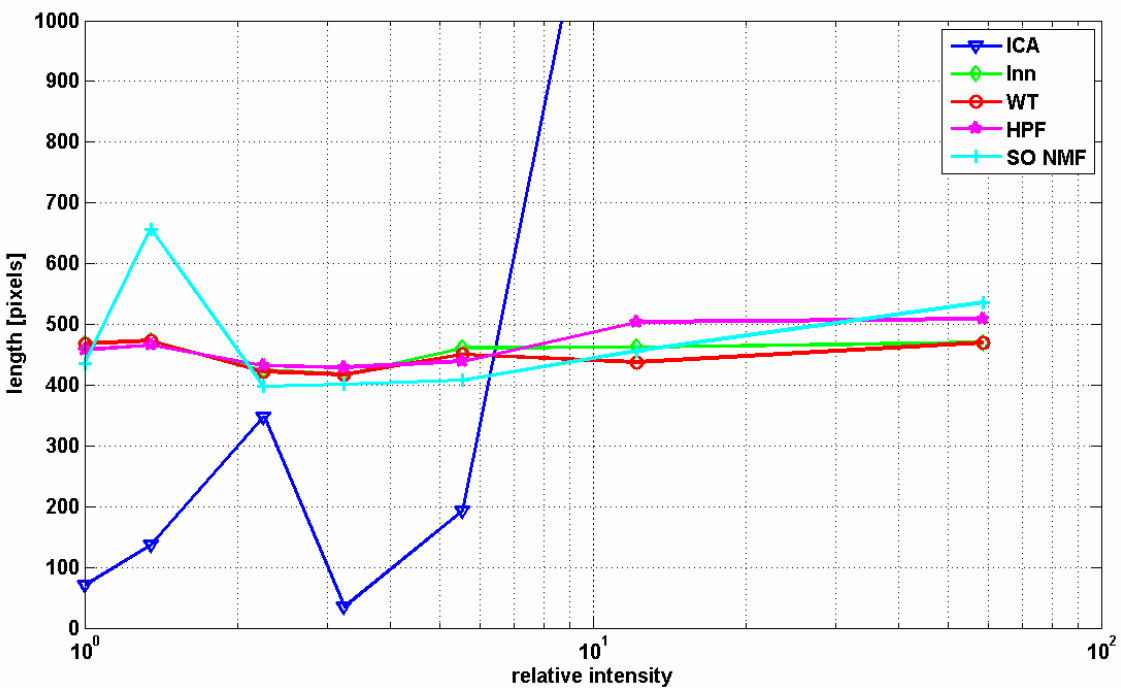

Fig. 4. Estimated lengths of the demarcation lines in pixels. Legend: dark blue triangles-ICA; green diamonds - DCA Inn; red circles - DCA WT; magenta stars - DCA HPF; sky blue triangles - SO NMF algorithm.

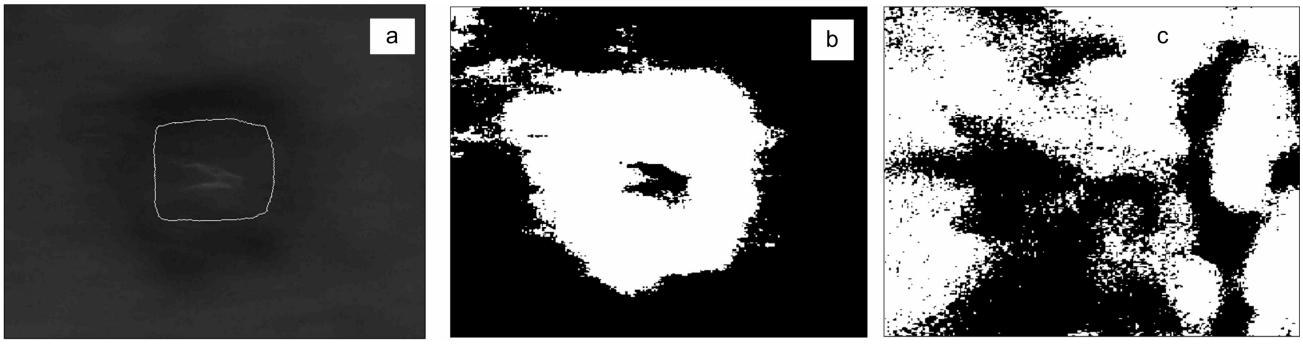

Fig. 5. (a) Demarcation line calculated by applying the level set clustering algorithm on the image shown in Fig. 1a; (b) and (c) spatial maps extracted from fluorescent RGB images shown in Figures 1a and 1c by means of K-means clustering algorithm with interclass distance parameter set to 45.

4. CONCLUSION

We have presented novel approach for robust demarcation of the skin tumors: unsupervised image segmentation methods the performance of which remains invariant under wide range of the variability of the fluorescence intensity. The approach exploits spectral diversity between the tumor and the surrounding skin in the recorded fluorescent multi-spectral RGB image. It is based on the recent extension of the ICA theory known under the common name of DCA. DCA is necessary to account for statistical dependence among the spatial maps of the tumor and surrounding tissue. Unlike several state-of-the art image segmentation methods, proposed DCA approach to tumor demarcation exhibited robust performance when intensity of the fluorescence has been varied almost two orders of magnitude. Such high level of robustness is a consequence of the scale invariance property of the used family of DCA algorithms.

ACKNOWLEDGEMENTS

The work of I. Kopriva and A. Peršin has been supported through grant 098-0982903-2558. The work of N. Puizina-Ivić and L. Mirić has been supported through grant 141-2180056-0481. Both grants were funded by the Ministry of Science, Education and Sport, Republic of Croatia.

REFERENCES

[1] Stenquist, B., Ericson, M.B., Strandeberg, C., Mölne, L., Rosén, A., Larkö, O. and Wennberg, A.M.,"Bispectral fluorescence imaging of aggressive basal cell carcinoma combined with histopathological mapping: a preliminary study indicating a possible adjunct to Mohs micrographic surgery," British J. of Dermatology 154, 305-309 (2006).

[2] English, D.R., Armstrong, B.K., Kicker, A. and Fleming, C., "Sunlight and cancer," Cancer Causes Control 8, 271-283 (1997).

[3] Ericson, M.B., Sandberg, C., Gudmundson, F., Rosén, A., Larkö, O. and Wennberg, A.M., "Fluorescence contrast and threshold limit: implications for photodynamic diagnosis of basal cell carcinoma," J. Photochem. Photobiol. B: Biol. 69, 121-127 (2003).

[4] Scott, M.A., Hopper, C., Sahota, A., Springett, R., Mcllroy, B.W., Bown, S.G. and. MacRobert, A.J., "Fluorescence Photodiagnostics and Photobleaching Studies of Cancerous Lesions using Ratio Imaging and Spectroscopic Techniques," Lasers Med Sci 15, 63-72 (2000).

[5] Bäumler, W., Abels, C. and Szeimies, R.M., "Fluorescence Diagnosis and Photodynamic Therapy in Dermatology," Med. Laser Appl. 18, 47-56 (2003).

[6] Fischer, F., Dickson, E.F., Pottier, R.H. and Wieland, H., "An Affordable, Portable Fluorescence Imaging Device for Skin Lesion Detection Using a Dual Wavelength Approach for Image Contrast Enhancement and Aminolaevulinic Acid-induced Protoporphyrin IX. Part. I Design, Spectral and Spatial Characteristics," Lasers Med Sci 16, 199-206 (2001).

[7] Fischer, F., Dickson, E.F., Kennedy, J.C. and Pottier, R.H., "An Affordable, Portable Fluorescence Imaging Device for Skin Lesion Detection Using a Dual Wavelength Approach for Image Contrast Enhancement and Aminolaevulinic Acid-induced Protoporphyrin IX. Part II. In Vivo Testing," Lasers Med Sci 16, 207-212 (2001).

[8] Ehrhardt, A., Stepp, H., Irion, K.M., Stummer, M., Zaak, D., Baumgartner, R. and Hofstetter, A., "Fluorescence Detection of Human Malignancies Using Incoherent Light Systems," Med. Laser Appl. 18, 27-35 (2003).

[9] Koenig, F., Knittel, J. and Stepp, H., "Diagnostic Cancer in Vivo," Science 292, 1401-1403 (2001).

[10] Hewett, J., Nadeau, V., Ferguson, J., Moseley, H., Ibbotson, S., Allen, J.W., Sibbett, W. and Padgett, M., "The Application of a Compact Multispectral Imaging System with Integrated Excitation Source to *In vivo* Monitoring of Fluorescence During Topical Photodynamic Therapy of Superficial Skin Cancers," Photochem. Photobiol. 73, 278-282 (2001).

[11] Kopriva, I., Peršin, A., Zorc, H., Pašić, A., Liopozenčić, J., Kostović, K. and Lončarić, M., "Visualisation of basal cell carcinoma by fluorescence diagnosis and independent component analysis," Photodiagnosis and Photodynamic Therapy 4, 190-196 (2007).

[12] Hyvärinen, A., Karhunen, J. and Oja, E., [Independent Component Analysis], Wiley Interscience (2001).

[13] Cichocki, A. and Amari, S., [Adaptive Blind Signal and Image Processing], John Wiley, New York (2002).

[14] Du, Q., Kopriva, I. and Szu, H., "Independent Component Analysis for Hyperspectral Remote Sensing," Opt. Eng. 45, 017008-1-13 (2006).

[15] Du, Q., Kopriva, I. and Szu, H., "Independent Component Analysis for Classifying Multispectral Images with Dimensionality Limitation," Int. J. Inf. Acq. 1, 201-216 (2004).

[16] Barros, A.K., [Advances in Independent Component Analysis], Springer, 63-71 (2000).

[17] Hyvärinen, A., "Independent component analysis for time-dependent stochastic processes," Proc. of the International Conference on Artificial Neural Networks (ICANN'98), 541-546 (1998).

[18] Kopriva, I. and Seršić, D., "Wavelet Packets Approach to Blind Separation of Statistically Dependent Sources," Neurocomputing 71, 1642-1655 (2008).

[19] Kopriva, I. and Seršić, D., "Robust Blind Separation of Statistically Dependent Sources Using Dual Tree Wavelets," Proc. of the 2007 IEEE International Conference on Image Processing, 433-436 (2007).

[20] Cichocki, A. and Georgiev, P., "Blind source separation algorithms with matrix constraints," IEICE Trans. on Fund. of Electr., Comm. and Comp. Sci. E86-A, 522-531 (2003).
[21] Tanaka, T. and Cichocki, A., "Subband decomposition independent component analysis and new performance criteria," Proc. of the IEEE Conference Acoustics, Speech and Signal Processing, 541-544 (2004).
[22] Adams, J.B. and Smith, M.O., "Spectral mixture modeling: A new analysis of rock and soil types at the Viking Lander 1 suite," J. of Geophys. Res. 91, 8098-8112 (1986).
[23] Adams, J.B., Smith, M.O. and Gillespie, A.R., [Remote Geochemical Analysis: Elemental and Mineralogical Composition], Cambridge University Press, 145-166 (1993).
[24] Settle, J.J. and Drake, N.A., "Linear mixing and estimation of ground cover proportions," Int. J. of Remote Sensing 14, 1159-1177 (1993).
[25] Chang, C.-I., Chiang, S.-S., Smith, J.A. and Ginsberg, I.W., "Linear spectral random mixture analysis for hyperspectral imagery," IEEE Trans.on Geosc. and Rem. Sens. 40, 375-392 (2002).
[26] Koldovský, Z., Tichavský, P. and Oja, E., "Efficient Variant of Algorithm for FastICA for Independent Component Analysis Attaining the Cramér-Rao Lower Bound," IEEE Tr. on Neural Networks 17, 1265-1277 (2006).
[27] Hyvärinen, A. and Oja, E., "A fast fixed-point algorithm for independent component analysis," Neural Computation 9, 1483-1492 (1997).
[28] Hyvärinen, A., "Fast and robust fixed-point algorithms for independent component analysis," IEEE Trans. Neural Network 10, 626-634 (1999).
[29] Lee, D.D. and Seung, H.S., "Learning the parts of objects by non-negative matrix factorization," Nature 401, 788-791 (1999).
[30] Cichocki, A., Zdunek, R. and Amari, S., "Nonnegative Matrix and Tensor Factorization," IEEE Sig. Proc. Magazine 25, 142-145 (2008).
[31] Zdunek, R. and Cichocki, A., "Nonnegative matrix factorization with constrained second-order optimization," Sig. Proc. 87, 1904-1916 (2007).
[32] Hoyer, P.O., "Non-negative Matrix Factorization with Sparseness Constraints," J. of Mach. Learn. Res. 5, 1457-1469 (2004).
[33] Li, Ch., Xu, Ch., Gui, Ch. and Fox, M.D., "Level Set Evolution Without Re-initilaization: A New Variational Formulation," Proc. IEEE International Conference on Computer Vision and Pattern Recognition, 430-436 (2005).
[34] http://www.mathworks.com/matlabcentral/fileexchange/loadCategory.do
[35] Bishop, C.M., [Pattern Recognition and Machine Learning], Springer, 423-460 (2006).